Fully Printed Stretchable and Multifunctional E-Textiles for Aesthetic Wearable Electronic Systems

Bin Tian, Yuhui Fang, Jing Liang, Ke Zheng, Panwang Guo, Xinyu Zhang, Youfusheng Wu, Qun Liu, Zhida Huang, Changyong Cao,* and Wei Wu*

Electronic textiles (e-textiles) that combine the wearing comfort of textiles and the functionality of soft electronics are highly demanded in wearable applications. However, fabricating robust high-performance stretchable e-textiles with good abrasion resistance and high-resolution aesthetic patterns for high-throughput manufacturing and practical applications remains challenging. Herein, the authors report a new multifunctional e-textile fabricated via screen printing of the water-based silver fractal dendrites conductive ink. The as-fabricated e-textiles spray-coated with the invisible waterproofing agent exhibit superior flexibility, water resistance, wearing comfort, air permeability, and abrasion resistance, achieving a low sheet resistance of 0.088 Ω sq^{-1}, high stretchability of up to 154%, and excellent dynamic stability for over 1000 cyclic testing ($\varepsilon = 100\%$). The printed e-textiles can be explored as strain sensors and ultralow voltage-driven Joule heaters driven for personalized thermal management. They finally demonstrate an integrated aesthetic smart clothing made of their multifunctional e-textiles for human motion detection and body-temperature management. The printed e-textiles provide new opportunities for developing novel wearable electronics and smart clothing for future commercial applications.

1. Introduction

Wearable electronics have attracted increasing attention due to their great potential in human motion tracking,[1,2] real-time health monitoring,[3,4] personalized healthcare,[5,6] human–machine interfaces,[7] and virtual/augmented reality.[8,9] Most flexible wearable electronic devices are fabricated with polymer or elastomer substrates which are uncomfortable to wear in direct contact with human skin.[10] As one of the most available

cloth materials, textiles are an ideal substrate for flexible wearable electronics due to their outstanding mechanical properties, good flexibility and softness, conformal contact with skin, and excellent wearing comfort.[11,12] Therefore, it is highly desirable to develop new smart electronic textiles (e-textiles) that can integrate the functionality of electronics and the comfort of textiles.[13,14] In particular, a facile, low-cost, and high-throughput manufacturing method for the fabrication of robust and reliable e-textiles is essential to future commercial applications of a variety of wearable electronics.

Currently, there are two major approaches in fabricating e-textiles: i) weaving or integrating electronic fibers made by wet spinning into textiles;[15–17] and ii) depositing conductive materials onto textile surfaces.[18–20] Coating methods such as spray-coating and dip coating, have the advantages of simplicity, fast, and low cost, and are the most commonly used methods for depositing conductive materials on textiles.[2,21] However, they are constraint by the entire surface deposition and cannot be patterned with aesthetic design.[22] The as-prepared e-textiles with this method need to be further integrated into clothing for real wearable applications.[23,24] Textile printing is widely used in the clothing industry for pattern decoration by directly screen-printing various inks onto the clothes.[25,26] Screen printing is another simple, fast, low-cost, and high-throughput fabrication technology. With a tailored new conductive ink and high-resolution screen-printing plate, it is expected to achieve a low-cost and mass production of printed e-textiles that has both electronics functionality and visual aesthetics. However, recent research on printed e-textiles has paid little attention to the aesthetics of printed electronics and the lack of high-resolution patterns for aesthetic designs also limits the development of smart clothing.[27,28]

On the other hand, the stretchability of e-textiles is extremely important for wearable applications because human body motion and deformation may generate a tensile strain as large as 55% in normal daily activities.[29] Most reported printed e-textiles only demonstrated good flexibility but very low stretchability due to the cracking of conductive layers printed on the textile.[28,30–32] Recently, Someya et al. fabricated a printed e-textile with a stretchability of up to 450% by adjusting

B. Tian, J. Liang, K. Zheng, P. Guo, X. Zhang, Y. Wu, Q. Liu, W. Wu
Laboratory of Printable Functional Materials and Printed Electronics
School of Printing and Packaging
Wuhan University
Wuhan 430072, China
E-mail: weiwu@whu.edu.cn
Y. Fang, Z. Huang, C. Cao
Laboratory for Soft Machines & Electronics
Department of Mechanical & Aerospace Engineering
Case Western Reserve University
Cleveland, OH 44106, USA
E-mail: ccao@case.edu

the solvent in conductive ink to control the penetration depth of ink into the textile.[33] However, such a method could not form a desired pattern on the fabrics because of the expansion and penetration of ink into the textile, and the stretchability of the e-textile also depended on the type and the woven structure of the textile. Obviously, it is still challenging to formulate suitable conductive screen-printing inks with satisfactory printability and versatility for e-textiles with excellent mechanical stretchability and electrical performance. In addition, the adhesion strength between the printed conductive layer and the fabric of the e-textile is also very important for practical applications but has not been well addressed.

In this article, we report a new water-based conductive ink made of silver fractal dendrites (Ag-FD) and a transparent binder (i.e., high-elasticity adhesive cement, HEAC). Using the screen printing method, the water-based conductive ink is deposited onto the textile surface in desired patterns, and then a thin layer of invisible waterproofing agent (IWA) is spray-coated on top of the conductive layer to prevent the electrodes from cracking. The as-printed e-textile exhibits excellent electrical properties, high stretchability, good water resistance, outstanding abrasion resistance, and excellent dynamic stability as well as wearing comfort. The printed e-textiles also exhibit excellent strain sensing performance and Joule heating performance. Thus, we finally demonstrated smart clothing made of the functional e-textiles for monitoring human motions and manage body temperature. We also demonstrate the composability of the new inks and fabrication methods to build stable printed e-textiles using a variety of substrate materials in a low-cost and scalable manner.

2. Results and Discussion
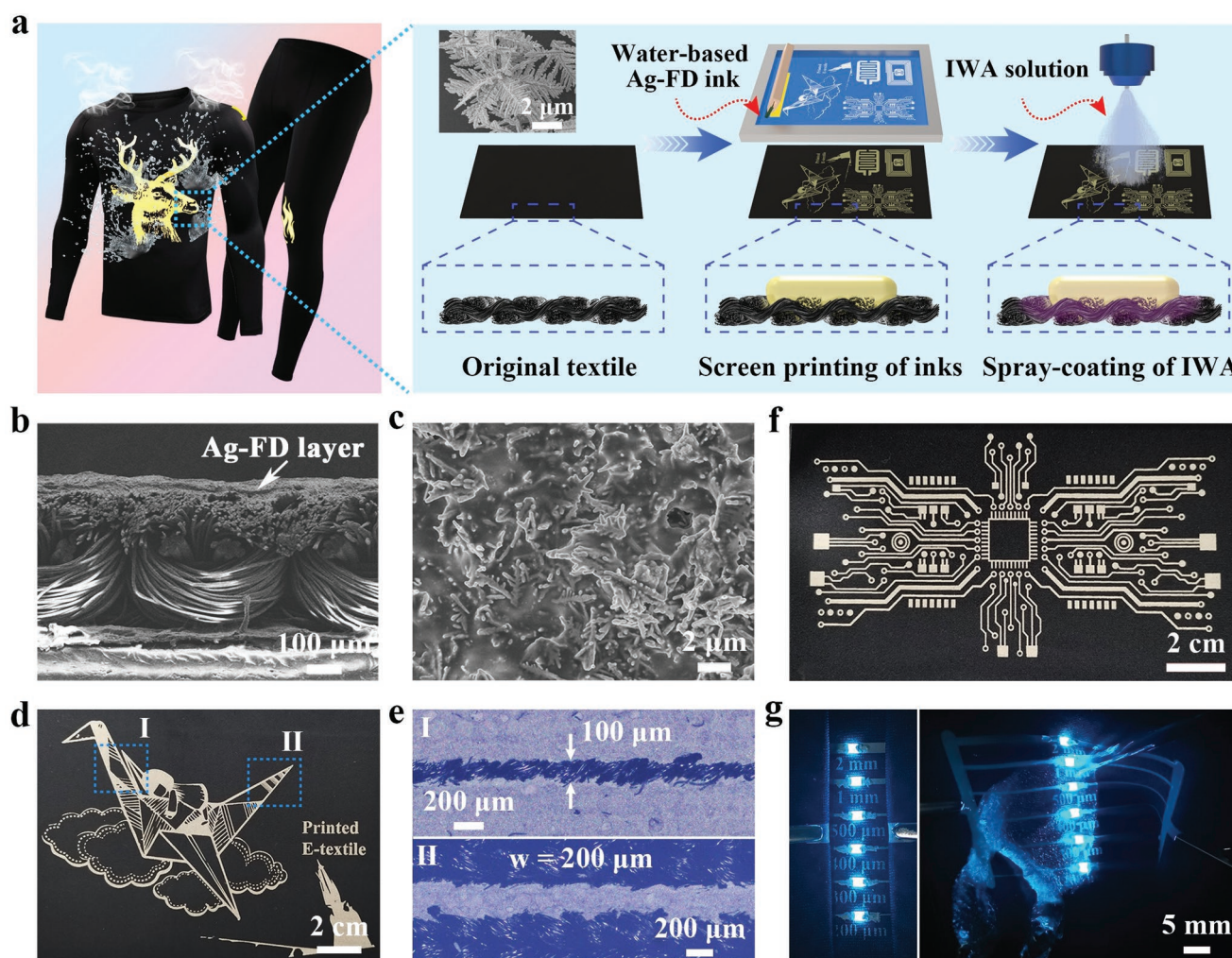
2.1. Design and Fabrication of the Printed e-Textiles

Figure 1a illustrates the fabrication process of using water-based Ag-FD conductive ink to create a new type of printed e-textiles with the merits of being waterproof, breathable, and aesthetic. Briefly, we first screen-print the water-based Ag-FD ink onto the surface of a piece of textile cut from a sport tight to form a conductive electrode layer. Then, we spray-coat a thin layer of IWA onto the printed Ag-FD conductive layer on the textile for a few times to obtain the final stretchable and water-proof e-textile. The water-based conductive ink consists of Ag-FD, HEAC, and a mixed solvent (Figure S1, Supporting Information). The conductive Ag-FD filler with unique 3D dendritic hierarchical structures (see the inset of Figure 1a) can easily contact one another to form a percolation network after printing, especially at the 3D spatial scale (Figure S2, Supporting Information).[34] The synthesis method of Ag-FD is simple and fast, enabling high-throughput manufacturing, and has the great potential for future commercialization. The uniformity and purity of the synthesized Ag-FD are verified by scanning electron microscopy (SEM) and X-ray diffraction (XRD) (Figure S3, Supporting Information). A commercialized fabric printing mucilage HEAC is used as the binder because of its high elasticity and excellent film-forming properties. To make the ink stable and compatible with the fabrication process, a mixed

solvent that consists of ethanol absolute (boiling point, 78 °C), DI water (boiling point, 100 °C), and ethylene glycol (boiling point, 197.3 °C) is used to disperse Ag-FD and dissolve the binder. We then spray-coat a thin layer of IWA, an organic silicon water-based waterproofing agent, to form a transparent waterproof layer on the surface of the printed e-textile for improving the mechanical and electrical properties under large strains.

The screen-printed water-based Ag-FD ink on the surface of the textile forms a dense interconnected Ag-FD thin film (Figure 1b,c and Figure S4, Supporting Information). The interconnected Ag-FD network is well embedded in the HEAC, resulting in a "brick-and-mortar" structure, in which HEAC serves as the "mortar" and Ag-FDs works as the "brick". With the loose fibers on the textile surface (Figures S5a and S5b, Supporting Information), the water-based conductive ink can penetrate into the textile to form an interwoven structure with the loose fibers (Figure S5c, Supporting Information). This "brick-and-mortar" structure and the strong interaction between the Ag-FD film and the loose fibers lead to the excellent adhesion of the Ag-FD thin film on the textile. XRD analysis confirms the deposition of Ag-FD conductive ink on the textile and there is no change of the composition in printed e-textiles after the spray-coating of IWA (Figure S6, Supporting Information). Figure 1d shows the printed conductive pattern for e-textiles, demonstrating that the new ink and printing process can achieve high resolution (≈100 µm, Figure 1e) and aesthetic design required for functional clothing. We also demonstrate that with optimized ink reception, different kinds of electrical electrodes and circuit patterns can be easily printed on textiles for a wide range of applications (Figure 1f and Figure S7, Supporting Information). More importantly, the printed e-textiles can survive under large strain conditions including bending, twisting, folding, and even immersing in water for 30 min (Figure 1g, and Figure S8 and Video S1, Supporting Information), demonstrating good flexibility and excellent water-resistance of the printed e-textiles.

2.2. Characterization of the Conductive Inks and Printed e-Textiles

The water-based Ag-FD conductive ink used for screen printing has to be optimized to ensure the good electrical and mechanical properties of the printed e-textile. As shown in **Figure 2**a, we formulate four different water-based Ag-FD conductive inks (labeled as Ink-25, Ink-35, Ink-45, and Ink-55) by adjusting the percentages of HEAC and the mixed solvent. Ink-25 and Ink-35 have severe precipitation after standing for 12 h, while Ink-45 and Ink-55 remain stable for a long time. This phenomenon indicates that the formulated conductive ink becomes more stable with the increases of HEAC content. The rheological properties of the ink such as viscosity, shear-thinning behavior, and thixotropy have significant impact on the quality of printed patterns. The viscosities of Ink-25, Ink-35, Ink-45, and Ink-55 measured at a shear rate of 0.1 s^{-1} are respectively 0.88, 21.54, 55.25, and 212.15 Pa s (Figure 2b), within the suitable range (0.05–500 Pa s) for screen printing.[35] In addition, all the four inks exhibit shear thinning behavior, thereby they can easily pass through the holes of the screen plate under the

Figure 1. Printed e-textile via water-based Ag-FD conductive ink. a) Schematic illustration of the main structure of a printed stretchable aesthetic e-textile and its fabrication process with customized patterns. b) SEM image of the printed Ag-FD conductive layer on a textile substrate. c) SEM image of the sectional view of the printed e-textile. d) Photograph of a printed aesthetic e-textile with exquisite conductive patterns. e) Optical images of printed conductive line pattern with a resolution of 100 μm. f) Photograph of an e-textile printed with a dense conductive circuit pattern for a chip. g) Photographs of a printed e-textile with integrated LEDs working at a folding state (left) and underwater (right). The conductive lines have the width of 0.2, 0.3, 0.4, 0.5, 1.0, and 2.0 mm, respectively.

squeezing motion of the squeegee. The good thixotropy of the ink is examined using a three-stage test method, from which we can observe that the viscosities of the inks decrease sharply when the shear rate increases from 0.1 to 200 s^{-1}, and return to their initial values when the shear rate goes back to 0.1 s^{-1} (Figure 2c). The desired rheological properties of the inks together with the good water absorption of the textile ensure a high quality of pattern printing on the textiles (Figure S9a–d, Supporting Information).

Both the ink ratio and the IWA coating have significant effects on the electrical and mechanical properties of the printed e-textiles. As shown in Figure 2d, the sheet resistance of the printed e-textiles without spray-coated IWA increases from 123.9 mΩ sq^{-1} to 312.6 mΩ sq^{-1} with the increase of the HEAC percentage from 35% to 55%, except for the Ink-25 (351.9 mΩ sq^{-1}). The result are mainly due to the wrapping effect of the conductive Ag-FD by the more insulating HEAC (Figure S10,

Supporting Information). The large sheet resistance of printed e-textile with Ink-25 is attributed to the less connected Ag-FD network induced by the lower Ag-FD loading and smaller viscosity of the ink (Figure S10a, Supporting Information). After spray-coating a thin layer of IWA, all the sheet resistances of the printed e-textiles have dramatically decreased. For example, the sheet resistance of the printed e-textile via Ink-35 reduces by ≈43.1% while the sheet resistance of the printed e-textile via Ink-45 reduces by ≈38.1% (Figure 2d).

On the other hand, the stretchability of printed e-textiles also increases with the HEAC percentage in the Ag-FD conductive ink (Figure 2e). The elasticity of the Ag-FD conductive layer on a textile increases with the increase of the HEAC percentage in the Ag-FD ink due to its good film forming ability and superior elasticity. The initial stretchabilities of the printed e-textiles via Ink-25, Ink-35, and Ink-45 are 42%, 66%, and 76%, respectively. After spray-coating a thin layer of IWA (e.g., spray coating ten
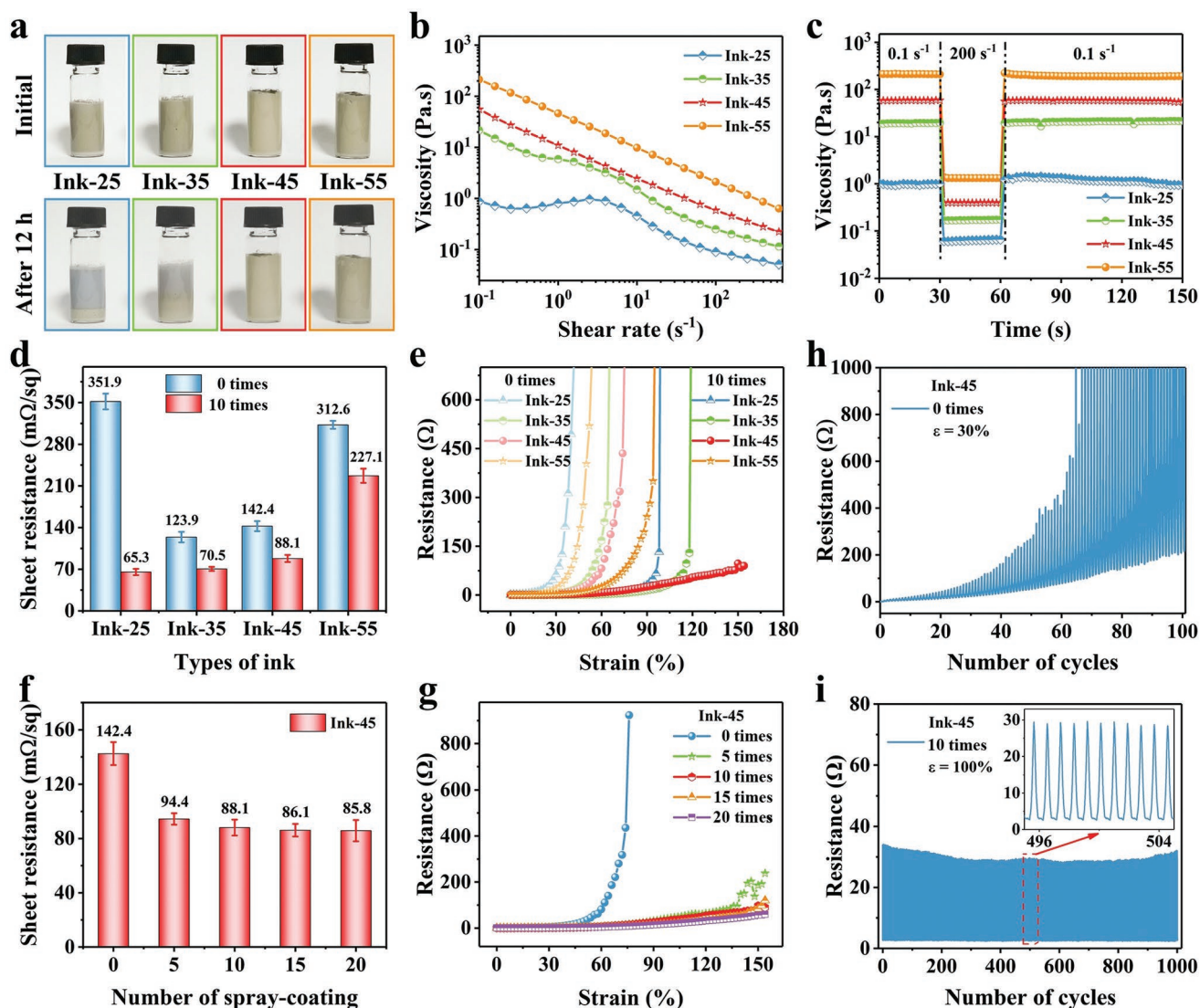
Figure 2. Characterization of the Ag-FD conductive inks and their electrical performance for printed electrodes. a) Photographs of the four different Ag-FD inks (Ink-25, Ink-35, Ink-45, and Ink-55) at their initial states and stored for 12 h. b) Variation of the viscosity of the four Ag-FD inks as a function of shear rate. c) Thixotropic behaviors of the four Ag-FD inks in screen printing. d) Comparison of the measured sheet resistance of the printed e-textiles using different Ag-FD inks. e) The electrical resistance of the printed e-textiles with different Ag-FD inks when subjected to different applied strains. The data of the printed e-textiles spray-coated with an IWA multiple times is also compared. f) Comparison of the measured sheet resistance of the printed e-textiles via Ag-FD Ink-45 after spray-coating different times of IWA. g) Variation of the electrical resistance of the printed e-textiles via Ag-FD Ink-45 after spray-coating different times of IWA as a function of applied strain. h) The electrical resistance of the printed e-textile via Ag-FD Ink-45 without spray-coating during 100 cycles of stretching/relaxation from 0% to 30% strain. i) Electrical resistance of the printed e-textile via Ag-FD Ink-45 spray-coated with IWA ten times during 1000 cycles of stretching/relaxation from 0% and 100% strain.

times), the stretchabilities of the three printed e-textiles are significantly increased to 98%, 118%, and 154%, respectively. We also find that the sheet resistance of the printed e-textiles reduces with an increasing number of spray coatings of the IWA. As shown in Figure 2f, for a specifically printed e-textile, the sheet resistance decreases from 142.4 mΩ sq^{-1} to 85.8 mΩ sq^{-1} when the number of coatings increases from 0 to 20 times. This effect becomes more significant under large strain conditions. Without spray-coating of IWA, the stretchability of the printed e-textile is only ≈75%, while the stretchability of the printed e-textiles with spray-coating IWA five times can reach up to 154% (Figure 2g). However, the effect of the

IWA becomes negligible after 20 times of IWA spray coating. Furthermore, under a cyclic loading condition of 30% strain and without the IWA coating, the resistance of the printed e-textile via Ink-45 drops fast, resulting in more than 100 fold increase of the resistance after only 100 stretching/relaxation cycles (Figure 2h). On the contrary, the printed e-textiles with IWA coating demonstrate an extremely stable conductivity even subjected to a cyclic strain of 100% for 1000 times (Figure 2i).

As shown in **Figure 3**, the Ag-FD conductive layer on the printed e-textile from Ink-25 exhibits obvious cracks under a tensile strain of 50%, while the Ag-FD conductive layer based on Ink-35 shows only very few cracks even subjected to a tensile
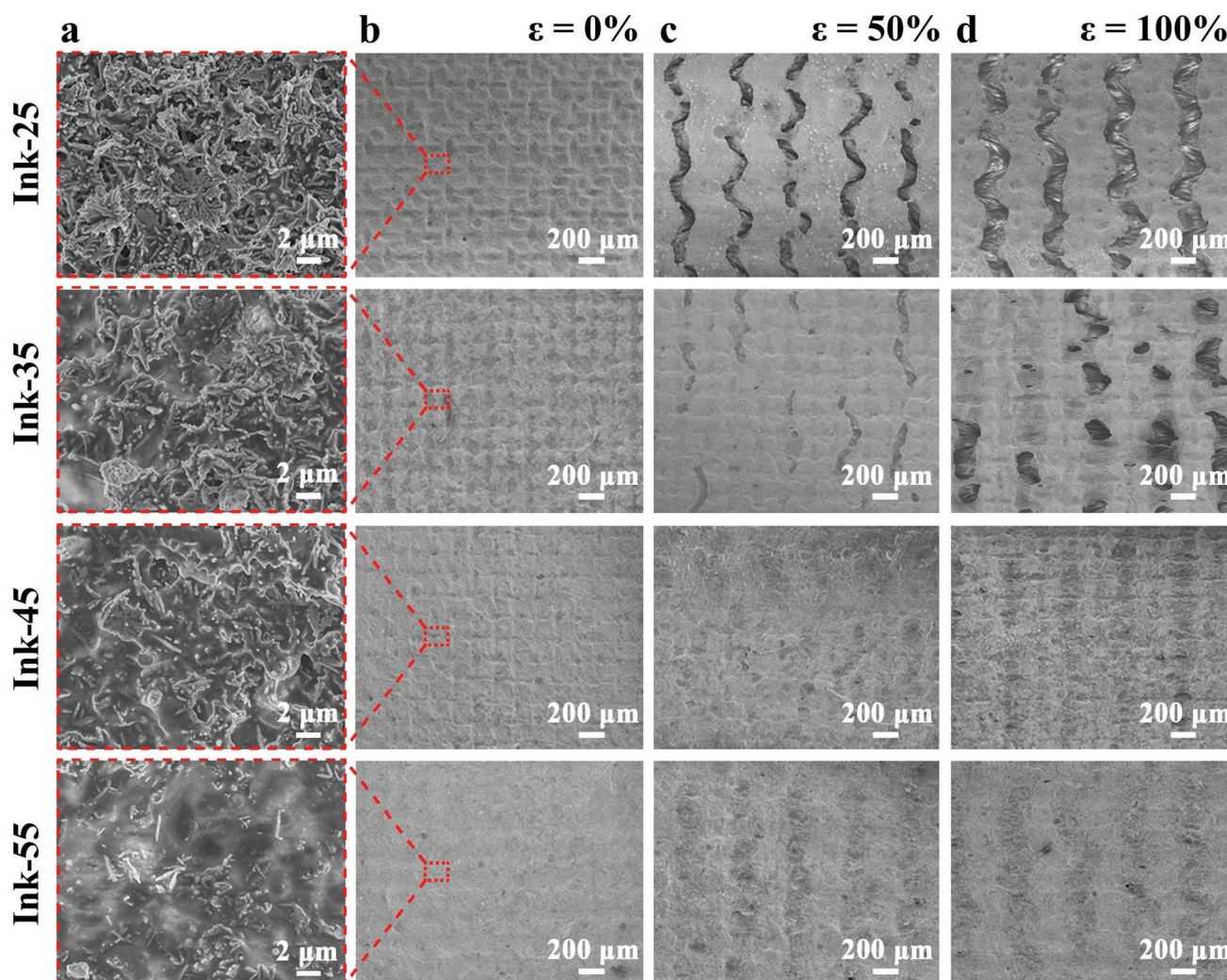
Figure 3. Surface morphologies of the printed Ag-FD thin films with different Ag-FD inks (Ink-25, Ink-35, Ink-45, and Ink-55) under different applied strains. The thin film is spray-coated with IWA for ten times. a) SEM images of the surfaces of the printed Ag-FD thin films. b–d) SEM images of the printed Ag-FD films on the textile surfaces when stretched to a strain of 0%, 50%, and 100%, respectively.

strain of 100%. There is no obvious crack that appeared in the printed e-textiles via Ink-45 and Ink-55 at an applied strain of 100%. The robustness to large strains may be attributed to the improved structural compaction between HEAC "mortar" and Ag-FDs "brick". When spray-coated on the surface of printed e-textiles, IWA can penetrate into the Ag-FD conductive layer to form a compact structure, thereby enhancing the interconnection between Ag-FDs and HEAC. As the number of spray-coating increases, more IWA is impregnated into the Ag-FD layer, resulting in the decrease of the resistance and the increase of the stretchability of printed e-textiles.

Figure 4a–c presents the SEM images of the original textile at the initial state, stretched state (150% strain), and restored state. The weave structure in textile makes it have heterogeneous properties in two distinct regions: weaving yarns (region I) and weaving gaps between the yarns (region II). When the textile sheet is stretched, the yarns are stretched slightly and the weave gaps are more significantly enlarged. After the disposition of a thin layer of an electrode (Figure 4d), the Ag-FD

conductive layer in the region II is more easily stretched subjected to an applied strain (Figure 4e). Once the applied strain is released, small wrinkles will be generated in the region II of the Ag-FD conductive layer on the textile (Figure 4f). Figure 4g shows the micro morphologies of the Ag-FD conductive layer at region I and region II respectively when the printed e-textile without spray-coating is stretched to 100%. It can be seen that a large amount of Ag-FD stacking and connections can be observed in region I while only a small amount of Ag-FD can be found in region II, resulting in less dense connections or increased resistance of the conductive layer on the e-textile. Remarkably, for the printed e-textile after spray-coating of IWA for ten times, we can still observe lots of Ag-FDs connected in region II even at 150% strain (Figure 4h). The results can explain the reason for the good mechanical stretchability and cyclic stability of the printed e-textile with a spray-coated IWA layer. It is concluded that the printed e-textiles via Ink-45 and spray-coated with IWA for ten times have demonstrated excellent electrical and mechanical
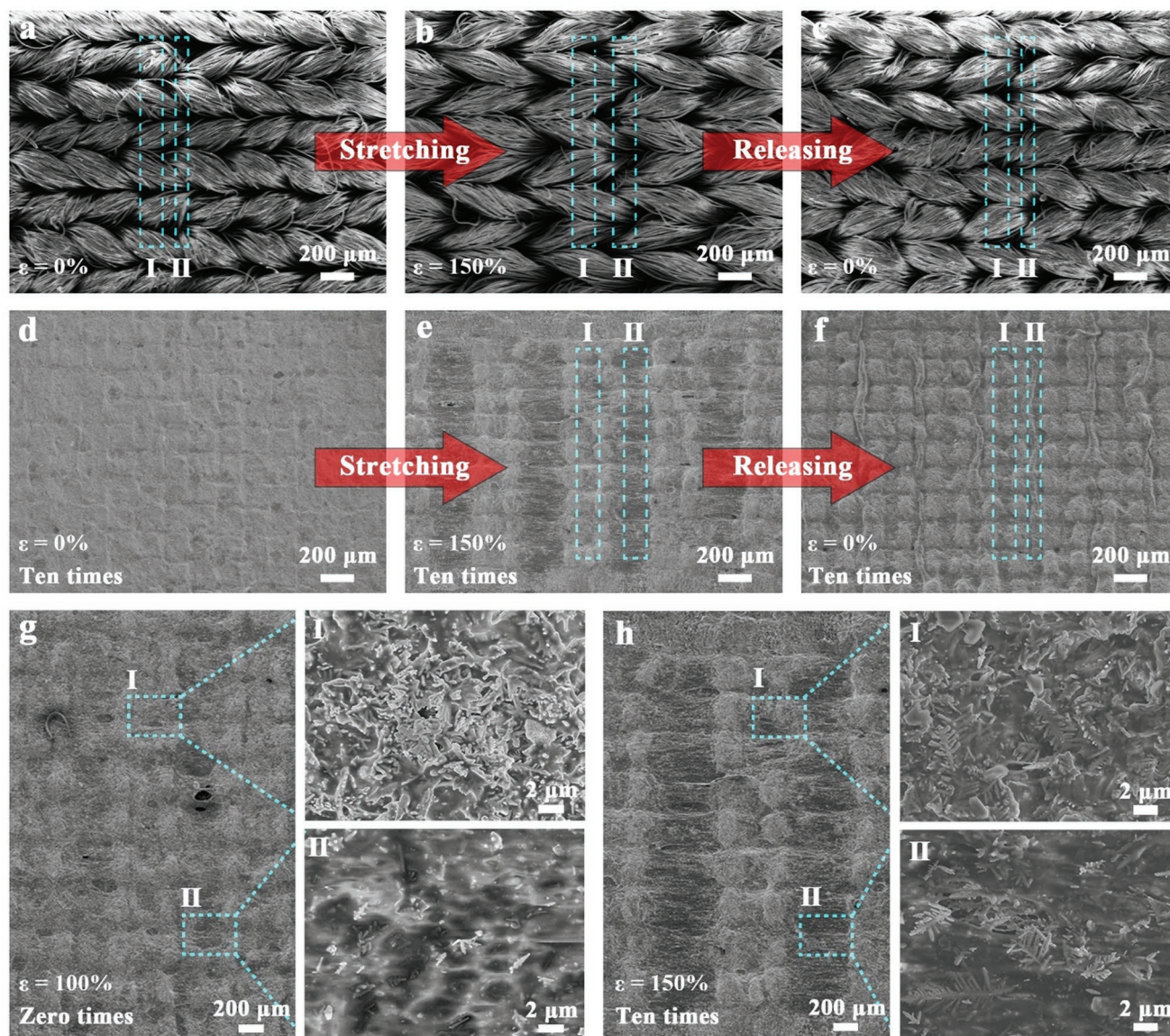
Figure 4. Surface evolution and stretchability mechanism of the printed Ag-FD thin films. SEM image of original textile at different strain states: a) 0%, b) 150%, and c) 0%. SEM image of the printed e-textile via Ag-FD Ink-45 after spray-coating IWA for ten times under different strains: d) 0%, e) 150%, and f) 0%. g) SEM images of the printed Ag-FD surface via Ag-FD Ink-45 without spray-coating IWA under a strain of 100%. h) SEM images of the printed Ag-FD surface via Ag-FD Ink-45 after spray-coating IWA ten times under a strain of 150%.

performance in wearable applications (Figure S11, Supporting Information). Therefore, in the following sections, all the printed e-textiles are fabricated using Ag-FD Ink-45 and spray-coating ten times of IWA unless otherwise stated.

We further characterized the water resistance, breathability, wear resistance, and washability of the printed e-textile as a wearable device. **Figure 5**a shows the wettability of printed e-textiles after spray-coating with IWA multiple times. It can be seen that the water contact angle of the Ag-FD conductive layer and the e-textile increased with the number of spray-coating. After ten times of coating, the contact angle becomes stable ($\approx133.0°$) in the hydrophobic condition. This phenomenon is attributed to the transparent waterproof layer formed by IWA

on the porous surface. Owing to the hydrophobicity of the e-textile, the printed circuits and electronic devices can work reliably with <20% change of relative resistance after soaking in deionized water for more than 24 h (Figure 5b). We also demonstrate that the electrical resistance of the printed e-textile also remains stable when immersed in synthetic perspiration for 24 h. Figure 5c presents the air permeability of the original textile, printed e-textile without IWA coating, and printed e-textile with IWA coating, which are 144.74, 95.79, and 95.21 L m^{-2} s^{-1}, respectively. The air permeability of the printed e-textile is slightly lower than that of the original textile due to the formation of an Ag-FD conductive layer. The adhesion strength of the printed layer on the textile is important

ADVANCED
SCIENCE NEWS
www.advancedsciencenews.com

NANO · MICRO
small
www.small-journal.com
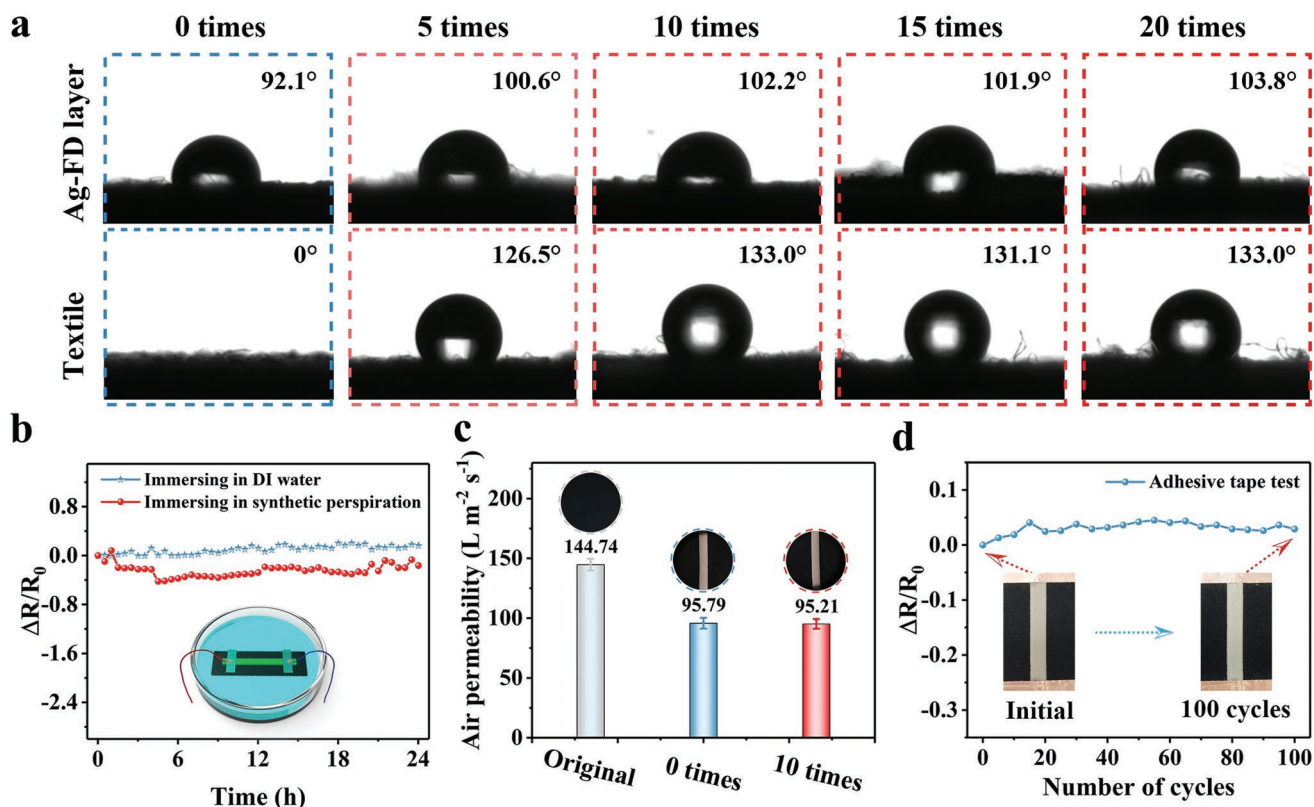
Figure 5. Water resistance, air permeability, and wear resistance characterization of the printed e-textiles. a) Variation of the water contact angle for the different numbers of spray-coating IWA on a printed e-textile. b) Relative resistance of a printed e-textile immersed in DI water and synthetic perspiration for 24 h. The inset is the schematic diagram of an e-textile immersed in liquid. c) Air permeability of the original textile, the printed e-textile without spray-coating, and the printed e-textile spray-coated with IWA ten times. d) Relative resistances of the initially printed e-textile and the printed e-textile with 1000 cycles of stretching/releasing from 0% and 100% strain when subjected to 100 cycles of adhesive tape testing. The insets are the photographs of as-printed e-textile and the printed e-textile experienced 100 cycles of adhesive tape testing.

for the durability of the final e-textile. From the tape testing, we find that the electrical resistance of the printed e-textile with spray-coated IWA coating remains very stable (i.e., only a slight increase of 3%) after 100 cycles of adhesive tape tests (Figure 5d). Even the printed e-textile after 1000 stretching/releasing cycles from 0% and 100% strain shows an electrical resistance change of only 9% after 100 cycles of adhesive tape tests, indicating a strong adhesion existing between the printed Ag-FD conductive layer and the textile. As shown in Figure S12, Supporting Information, after experienced up to 1000 abrasion tests, the electrical resistance of the printed e-textile has only increased by ≈68.3%, and can still keep a satisfactory conductivity based on its absolute value, verifying that the printed e-textile has good abrasion resistance. Due to its excellent water and abrasion resistance, the printed e-textile shows only ≈142.5% increase in electrical resistance after ten times of hand-washing tests, exhibiting excellent washability (Figure S13 and Video S3, Supporting Information). Furthermore, the printed e-textile also demonstrates outstanding thermal stability at a temperature of 60 °C (Figure S14, Supporting Information). These results demonstrate that the great potential of the printed e-textile for practical wearable applications that require good air permeability, excellent water resistance, and outstanding wear resistance and washability.

2.3. Strain Sensing Performance of the Printed e-Textiles

The printed e-textiles can be utilized as strain sensors to detect human motions in daily life. We fabricated a printed e-textile-based strain sensor (PESS) with a U-shaped pattern to evaluate its strain sensing performance. To obtain stable sensing performance, the PESSs is performed after 20 pre-stretching experiments under 60% strain and then kept under an ambient condition for 12 h. The measured data shows that the working strain range of the PESS can reach up to 155% (**Figure 6**a). The sensing curve of the PESS can be divided into two linear regions: 0–65% with the linearity of 0.943 and 70–155% with the linearity of 0.992. The gauge factors (GFs) in these two linear regions are 20.6 and 119.4, respectively, which are calculated by $GF = (R - R_0)/(R_0 \, \varepsilon)$ where R, R_0, and ε represent the real-time resistance, the initial resistance, and the applied strain. Moreover, the new PESS has a short response time of 214 ms under a strain of 55% at a strain rate of 60 mm s^{-1} (Figure 6b) and demonstrates stable sensing responses at different working frequencies of 0.25, 0.5, 0.75, and 1 Hz under the stretching/relaxation cycles between 0% to 20% strain (Figure 6c). In comparison with previous textile-based sensors reported in literature, the sensing performance of PESS is much better (**Table 1**).[15,23,31,36–39]
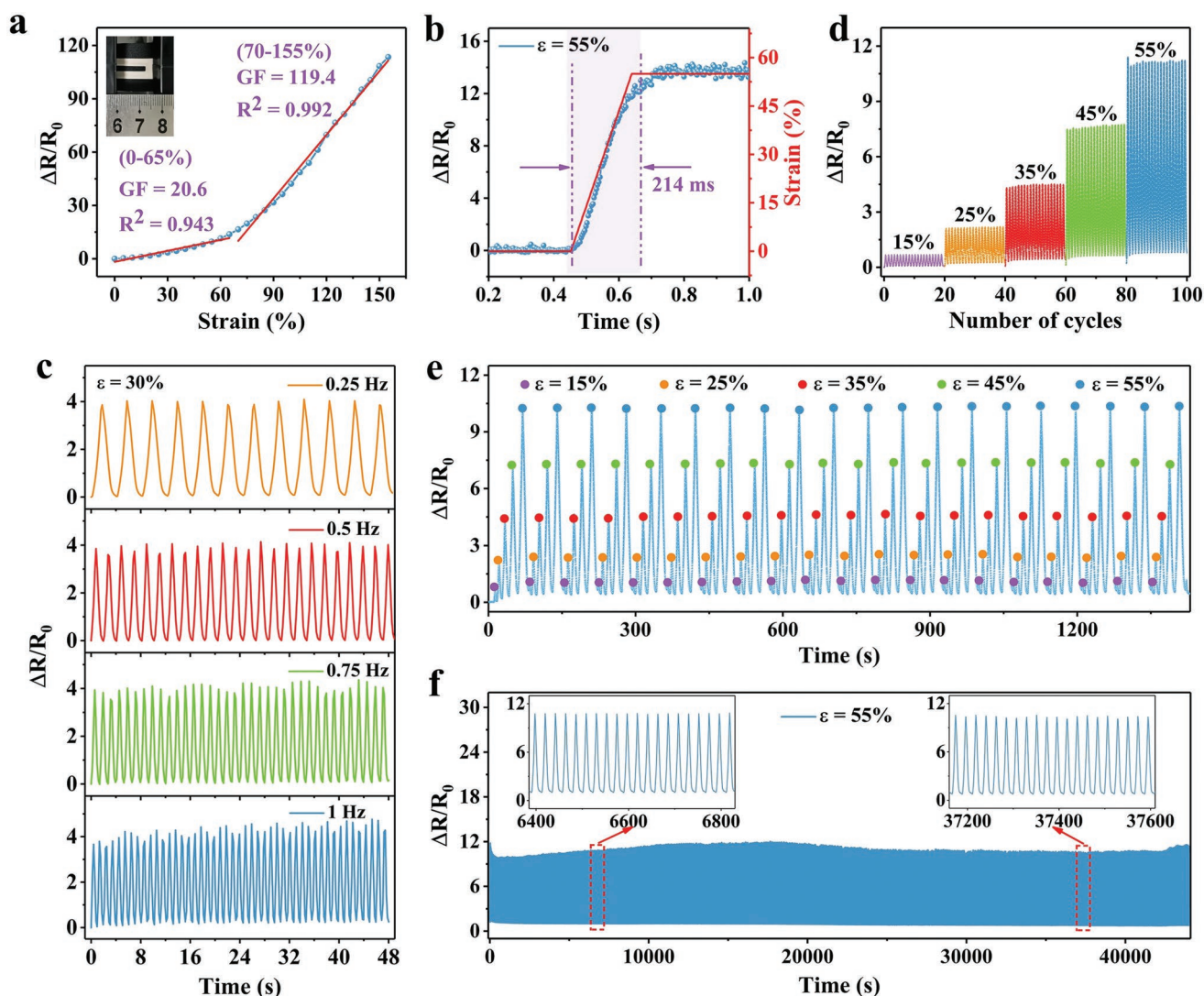
Figure 6. The sensing performance of the printed e-textile as strain sensors. a) The variation of the relative resistance of a PESS under different strains. b) The response time of a PESS under a strain of 55% at a strain rate of 60 mm s^{-1}. c) Relative resistance changes of the PESS at different stretching frequencies under a strain of 30%. d) Comparison of the relative resistances under various cyclic strains (15%, 25%, 35%, 45%, and 55%). e) Stability of the resistance change under a cyclic strain varying from 0% to 55%. f) Variation of the relative resistance change of the printed PESS in 2000 stretching/relaxation cycles between 0% and 55% strain.

We also test the stability and reliability of the PESS in dynamic sensing under a cyclic stretching/relaxation loading to different strain levels: 15%, 25%, 35%, 45%, and 55% (Figure 6d). Figure 6e shows that the PESS gives the same responses to a specific strain within the strain range of 0–55%, enabling accurate identification of specific motions or gestures. In more than 2000 cycles of stretching/relaxation test with an applied strain of 55%, the measured signals of PESS do not show obvious degradation in the shape and peak value of the electrical response (Figure 6f), indicating that the PESS has excellent dynamic stability and sensing performance when used as strain sensors for wearables. However, due to the viscoelasticity of HEAC and the interaction between Ag-FD and HEAC, the PESS exhibits obvious hysteresis behavior (Figure S15, Supporting Information), which is similar to the results of

polymer-based resistive strain sensors that have been reported.[40–42] According to the formula of the degree of hysteresis (DH):[43]

$$DH = \frac{A_{Stretching} - A_{Releasing}}{A_{Stretching}} \times 100\% \tag{1}$$

where $A_{Stretching}$ and $A_{Releasing}$ are the area of the stretching state curve and the area of the releasing state curve, respectively. The DH value of the PESS is about −13.5%.

2.4. Joule Heating Performance of the Printed e-Textiles

The printed e-textile can serve as a personalized thermal management unit for wearable use by converting electrical

Table 1. Comparison of the performance of printed e-textile with the reported data in literature.

Materials	Method	Aesthetic	Conductivity	Stretchability	Durability	Functions	Ref.
Conductive yarn	Pre-stretching + lockstitch	No	N/A	100%	2500 cycles (40%)	Strain sensing (GF = 7.5 [0–50%])	[15]
PPy/MXene	Dip coating	No	2.33 Ω sq^{-1}	N/A	1000 cycles (bending)	Water resistance, EMI shielding, Joule heating (79 °C/4 V)	[2]
Ag/PDA/CF	Dip coating	No	0.26 Ω sq^{-1}	N/A	500 cycles (bending)	Water resistance, Joule heating (53 °C/3 V)	[44]
MXene	Spray-drying coating	No	5 Ω sq^{-1}	N/A	5000 cycles (bending)	Strain sensing (GF = 2.08 [0.86–2.09%]), Joule heating (150 °C/6 V), EMI shielding	[36]
Commercial pen ink (CB)	Dip coating	Yes (by tailoring)	0.125 S m^{-1}	30%	5000 cycles (10%)	Strain sensing (GF = 62.9 [0–30%])	[45]
Ag NWs	Pre-stretching (30%) + laser scribing + heat press	No	0.2 Ω sq^{-1}	50%	15 cycles (50%)	Strain sensing, ECG and EMG sensing, wireless heating	[46]
Ppy/β-FeOOH	Dip coating + in-situ polymerization	No	0.308 KΩ (5 cm)	100%	1500 cycles (30%)	Water resistance, strain sensing (GF = 3.26 [20%]), Joule heating (50.4 °C/12 V)	[39]
PDMS/MXene/PDA	Dip-coating	No	126 S m^{-1}	140%	500 cycles (20%)	Water resistance, strain sensing (GF = 18 [5–30%]), Joule heating (60 °C/12 V), temperature sensing	[37]
MWCNTs	Stencil printing + electroless	No	0.284 Ω sq^{-1}	20%	150 cycles (0.5–2.5%)	Strain sensing (GF = 4 [<15%]), EMI shielding	[31]
CB	Mask printing	No	4.26 KΩ	130%	10 000 cycles (50%)	Water resistance, strain sensing (GF = 57 [130%])	[23]
Graphene	Screen printing	No	10.26 ± 1.5 S m^{-1}	5%	N/A	Strain sensing (GF = 30 [5%])	[38]
Ag-FD	Screen printing	Yes	0.088 Ω sq^{-1}	155%	1000 cycles (100%)	Water resistance, wear resistance, strain sensing, Joule heating	This work

energy into thermal energy. We print an e-textile-based Joule heater (PEJH) with a rectangular electrode having a honeycomb pattern and then connect it with an applied voltage through a direct current (DC) power supply (**Figure 7**a). Figure 7b,c shows the time-dependent temperature curves of the PEJH under different voltages. It can be seen that the saturation temperature of the PEJH monotonously increases with the applied voltage. There is a linear relationship with a slope of 101.9 °C cm^2 w^{-1} between the saturation temperature and the input power density for the PEJH (Figure 7d). The infrared (IR) thermal images confirm that the PEJH exhibits a uniform heating effect under different voltages from 0.6 to 1.6 V (Figure 7e). Moreover, the Joule heating performance of the PEJH is superior to previous textile-based Joule heaters reported in

literature (Table 1).[2,36,37,39,44] The demonstrated excellent heating performance of the PEJH enables the use of portable low-voltage batteries and thereby ensures the safety of the human in using wearable electronics.

Figure S16a, Supporting Information, shows the thermal performance of the PEJH under bending states with different bending radii. It is observed that the resistance of PEJH decreases with the decrease of the bending radius, thereby the saturation temperature at 1 V increasing from 105.5 °C at the initial flat state to 108.0 °C when the bending radius is 6 mm (Figure S16b, Supporting Information). The heating saturation temperature of the PEJH at 1 V can be kept in the range of 105 to 114 °C during 10 bending/relaxation cycles to a bending radius of 6 mm (Figure 7f and Video S4, Supporting

ADVANCED
SCIENCE NEWS
www.advancedsciencenews.com

NANO · MICRO
small
www.small-journal.com
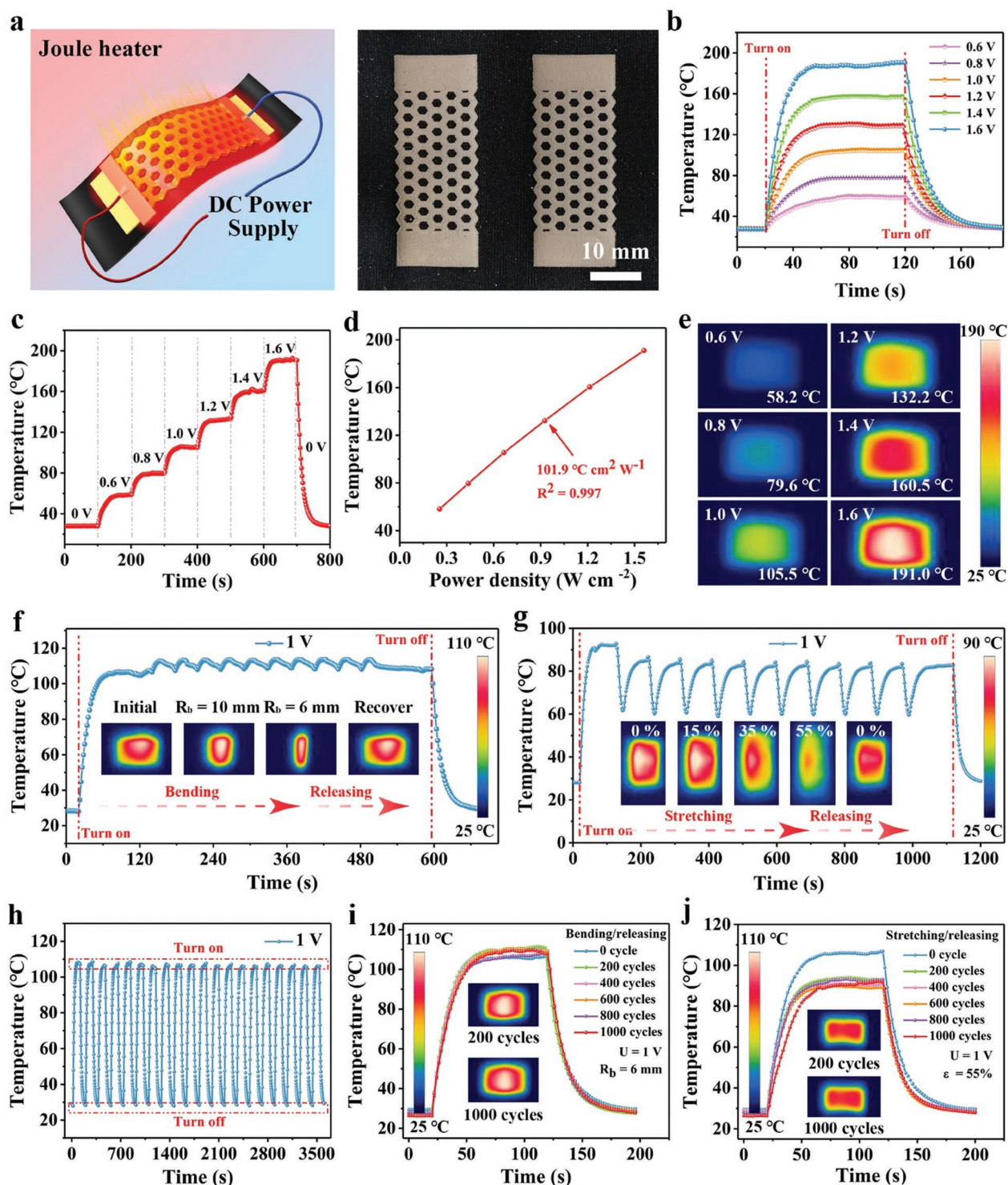
Figure 7. Evaluation of the printed e-textile as a Joule heater for wearables. a) Schematic diagram of the PEJH, consisting of the printed e-textile and a DC power supply. b) Temperature versus time curves of the PEJH at different applied voltages. c) The temperature change of the PEJH when the applied voltage increases from 0 to 1.6 V. d) Temperature versus power density curve of the PEJH. e) IR images of the PEJH under different applied voltages. f) The Joule heating performance of the PEJH during 10 bending/releasing cycles with a bending radius of 6 mm under an applied voltage of 1 V. The insets are the IR images of a PEJH in different bending states. g) The Joule heating performance of a PEJH in 10 stretching/releasing cycles varying from 0% to 55% strain under an applied voltage of 1 V. The insets are the IR images of the PEJH at different strain states. h) The temperature change of the PRJH in 20 heating/cooling cycles. i) Influence of the bending deformation on the heating performance of the PEJH. The bending radius is 6 mm and the applied voltage is 1 V. The insets are the IR images of the PEJH after 200 and 1000 cycles of bending/releasing. j) Influence of the stretching strain on the heating performance of the PEJH. The applied strain is varying from 0% and 55% and the applied voltage is 1 V. The insets are the IR images of the printed PEJH after 200 and 1000 cycles of stretching/releasing.

Information), indicating an excellent Joule heating performance under bending deformations.

We further demonstrated that the PEJH can work well under large tensile strains (Figure S17a, Supporting Information). As the strain increases, the resistance of PEJH increases, and the heating temperature at 1 V decreases from 105.9 °C in the initial state to 40.2 °C at the applied strain of 55% (Figure S17b, Supporting Information). During 10 cycles of stretching/releasing with an applied strain of 55%, the heating temperature of the PEJH fluctuates with the applied strain in the range of 60 to 90 °C under an applied voltage of 1 V (Figure 7g and Video S4, Supporting Information). This is because the electrical resistance of the PEJH increases/recovers as the strain is applied/released, which is consistent with our results shown in Figure 2. For long-term use, we demonstrate that the PEJH can maintain a stable temperature at 110 °C with an applied voltage of 1 V for 1 h (Figure S18, Supporting Information).

Moreover, the heating saturation temperature of the PEJH at 1 V can be stabilized at ≈108 °C during the 20 heating/cooling cycles of cyclic testing (Figure 7h). The stable heating performance of the PEJH under cyclic mechanical bending loads are also confirmed by the collapsed temperature–time curves of the PEJH for over 1000 times of bending test with a bending radius of 6 mm (Figure 7i and Figure S16c,d, Supporting Information). Although the electrical resistance of the PEJH increases by 38% after 1000 stretching/releasing cycles (applied strain ε = 55%), the PEJH can still be heated to 90.8 °C under a voltage of 1 V (Figure 7j and Figure S17c,d, Supporting Information). These results indicate that the printed e-textile can be used as Joule heaters for personalized thermal management for wearable applications such as cold protection and thermal therapy.

2.5. Evaluation of an Integrated Smart Clothing

As a proof-of-concept, we fabricate a set of aesthetic smart clothing (**Figure 8**a) for possible use in human body temperature control and motion monitoring. The aesthetic smart clothing is screen-printed with a series of conductive patterns, including polylines, a deer head, basketball players, and a fire flame. The polyline conductive pattern is used as a localized heater on the shoulder joint part of the smart clothing, which can be powered by an ultra-low voltage of 0.7 V. The temperature can be maintained at 40–60 °C in the relaxed state and the raised state of the shoulder (Figure 8b), which may be utilized for relieving shoulder pain. Meanwhile, it can also work as a motion sensor when the volunteer lifts up and puts down his hands repeatedly (Figure 8c). In physical training or excise, smart clothing can capture the motion patterns (e.g., barbell lifting) of the volunteer through the relative resistance change induced in the e-textile (Figure 8d and Video S5, Supporting Information). Remarkably, its performance will not be affected by the splashed water or sweat generated in physical excises. Additionally, the integrated smart clothing can also be used to monitor the different walking states of humans. For example, it can easily distinguish the differences between resting, slow/fast walking, and running by sensing the frequency of changes in relative resistance (Figure 8e and Video S5, Supporting Information). More importantly, the fabricating method and the tunable inks of printed e-textiles can be extended to other kinds of textile substrates (such as leather fabric, cotton fabric, and polyester fabric) in the state of bending and stretching up to a 100% strain (Figure S19, Supporting Information).

3. Conclusion

In summary, we have demonstrated a low-cost and scalable manufacturing method and effective conductive inks for fabricating stretchable, conductive, air-permeable, and water-proof e-textiles with excellent strain sensing and Joule heating. The new water-based Ag-FD conductive ink was formulated by mixing Ag-FD, HEAC, and a complex solvent made from absolute ethanol, ethylene glycol, and deionized water, and had the desired rheological properties. The effects of the ink components and the spray-coating of IWA on the electrical and mechanical properties of the printed e-textile were investigated in detail. The superior printed e-textile via Ink-45 showed a low sheet resistance of 0.88 mΩ sq^{-1}, high stretchability of 154%, and excellent dynamic stability after spray-coating with IWA. In addition, the strain sensors made of the printed e-textile exhibited a large sensing range of 155% and the thermal management unit made of the printed e-textile showed an outstanding Joule heating performance and good stability under different kinds of loading such as bending, stretching, and cyclic or long-time tests.

4. Experimental Section

Materials: Silver nitrate (Ag NO$_3$, AR), ethanol absolute (C$_2$H$_6$O), and ethylene glycol (C$_2$H$_6$O$_2$, AR) were purchased from Sinopharm Chemical Reagent Co., LTD. Hydroxylamine solution (H$_3$NO, 50 wt% in H$_2$O) was purchased from Sigma-Aldrich Co., LTD. HEAC was purchased from Jiangshan Color Printing Material Co., LTD (China). IWA was purchased from Nanjing Qiaojiang New Material Co., LTD (China). Sports tights (plain knitted fabric, composed of 86% polyester fiber and 14% spandex, with a number of warp yarns and weft yarns per inch of 51 and 68, and a thickness of 0.437 mm) was purchased from Jinjiang Yuanxiang Garment Weaving Co., LTD (China). The DI water (18.2 MΩ) was used throughout this whole experiment.

Synthesis of Ag-FD: The Ag-FD was prepared by a facile one-step redox reaction at ambient temperature and pressure conditions. The 1.02 g Ag NO$_3$ and 1450 μL hydroxylamine solution were dissolved in 75 mL DI water to form solutions A and B, respectively. Then, the two solutions were added dropwise at the same speed of 10–12 mL min^{-1} through constant pressure separatory funnels, and uniformly mixed and sufficiently reacted under a magnetic stirring of 600 rpm. After stirring for 20 min and then washing with DI water and ethanol absolute several times, the Ag-FD was obtained. The as-prepared Ag-FD was then dispersed in ethanol absolute for preparing the Ag-FD conductive inks.

Formulation of Ag-FD Conductive Inks: Water-based Ag-FD conductive inks were formulated by a wet mixing process, in which the conductive filler Ag-FD was not dried. First, the mixed solvent was prepared by uniformly mixing DI water, ethanol absolute, and ethylene glycol in a volume ratio of 1:2:2. Subsequently, the Ag-FD, HEAC, and mixed solvent were mixed and violently stirred by a handheld mixer F6/10 for 20 min to obtain a homogeneous water-based Ag-FD conductive ink. Four kinds of water-based Ag-FD conductive inks with different ink ratios were prepared and marked as Ink-25, Ink-35, Ink-45, and Ink-55, respectively. The weight ratios of Ag-FD: HEAC: mixed-solvent for the four inks are 25:25:50, 25:35:40, 25:45:30, and 25:55:20, respectively.
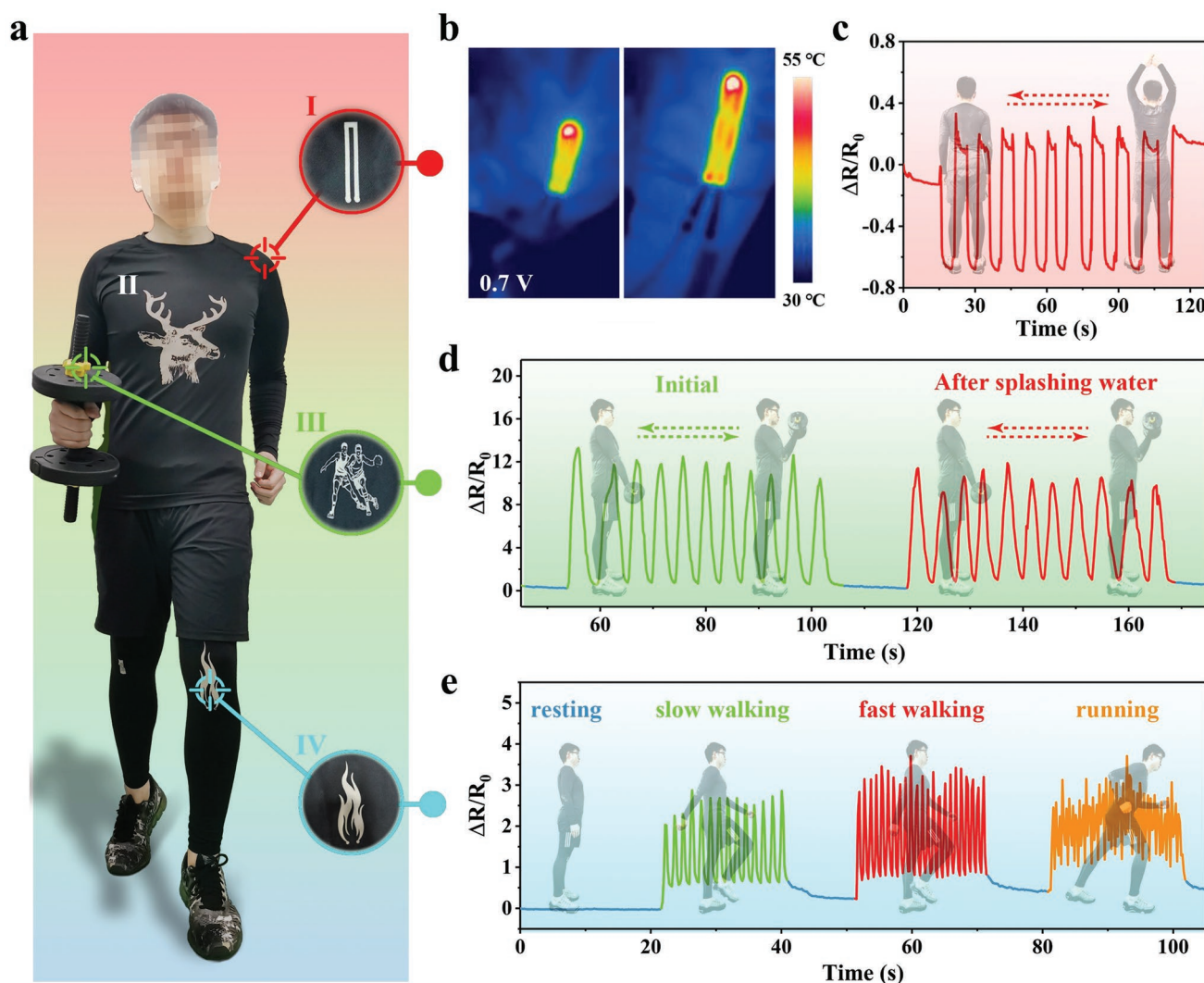
Figure 8. On-body evaluation of the fully printed aesthetic smart clothing. a) Photograph of the smart-clothing with a variety of printed aesthetic conductive patterns: polyline (I), deer head (II), basketball players (III), and fire flame (IV). b) The IR images of the smart clothing under an applied voltage of 0.7 V. c) The measured real-time relative resistance changes of the smart clothing when the volunteer lifts and puts down his hands repeatedly. d) The variation of the responsive signal obtained by the smart clothing when doing excises. The splashed water has little influence on the measured signals of smart clothing. e) Real-time monitoring of the human motion state using smart clothing: resting, slow walking, fast walking, and running.

Fabrication of the Printed e-Textiles with Customized Patterns: The printed e-textiles were fabricated by using a screen-printing method and a spray coating method. Sports tights were used as the textile substrate without further treatment. First, the as-prepared water-based Ag-FD conductive ink was screen-printed onto the textile substrate using a 150-mesh count screen plate (Figure S20, Supporting Information) to obtain the Ag-FD conductive layer. The number of screen-printing was three, and the Ag-FD conductive layer was dried at 100 °C for 1 min after each printing. After being dried at 140 °C for 20 min, the IWA was spray-coated several times onto the printed e-textile. Finally, the printed e-textile was placed in the air for 12 h to let the waterproofing agent fully penetrate into the Ag-FD conductive layer and the textile, followed by drying at 50 °C for 2 h to remove the residual solvent in the printed e-textiles.

Characterization and Measurement of the e-Textile: SEM was performed on a Hitachi S-4800 scanning electron microscope. The XRD pattern was recorded from 10° to 80° using a Bruker D8 advance X-ray Cu Kα radiation diffractometer. Optical images were taken by an Olympus

BX51 microscope. The rheological properties of Ag-FD inks were measured using a TA AR2000ex rotary rheometer. The sheet resistance of printed e-textiles was measured using an FP-001 four-probe resistance tester. Real-time resistance was recorded using a Keithley-2400 digital multimeter, and the motorized linear stage with a DY-IS stepper motor controller was utilized to apply strain. The water contact angle was recorded using a SL200IS contact angle analyzer (USA KINO Industry Co., Ltd). The air permeability was measured using a YG641E numerical air permeability tester (Ningbo Textile Instrument Factory). The tape adhesion test was performed by sticking a 3M tape on the surface of the printed e-textile and pressing it 20 times with an eraser. The abrasion test was performed by a YG401C fabric abrasion tester (Martindale, Ningbo Textile Instrument Factory, China) with an applied pressure of 9 KPa. The hand-washing test includes the following steps: I) immerse the printed e-textile into water; II) add washing powder and then vigorously knead the printed e-textile for ≈20 times; III) knead the printed e-textile for ≈20 times under water to remove the washing powder; and IV) dry the printed e-textile with a hairdryer (Video S3,

Supporting Information). The Joule heating performance was performed using a FLIR IR camera with a FLIR Tool+ analysis tool, and a PS-3005D DC power supply (ZHAOXIN) was used to apply the voltage.

Supporting Information

Supporting Information is available from the Wiley Online Library or from the author.

Acknowledgements

Conflict of Interest

The authors declare no conflict of interest.

Data Availability Statement

The data that support the findings of this study are available from the corresponding author upon reasonable request.

Keywords

[1] B. Tian, Q. Liu, C. Luo, Y. Feng, W. Wu, *Adv. Electron. Mater.* **2020**, *6*, 1900922.

[2] B. Tian, W. Yao, P. Zeng, X. Li, H. Wang, L. Liu, Y. Feng, C. Luo, W. Wu, *J. Mater. Chem. C* **2019**, *7*, 809.

[3] J. Kim, A. S. Campbell, B. E. de Avila, J. Wang, *Nat. Biotechnol.* **2019**, *37*, 389.

[4] S. M. A. Iqbal, I. Mahgoub, E. Du, M. A. Leavitt, W. Asghar, *npj Flexible Electron.* **2021**, *5*, 9.

[5] F. Ershad, A. Thukral, J. Yue, P. Comeaux, Y. Lu, H. Shim, K. Sim, N. I. Kim, Z. Rao, R. Guevara, L. Contreras, F. Pan, Y. Zhang, Y. S. Guan, P. Yang, X. Wang, P. Wang, X. Wu, C. Yu, *Nat. Commun.* **2020**, *11*, 3823.

[6] C. Tan, Z. Dong, Y. Li, H. Zhao, X. Huang, Z. Zhou, J. W. Jiang, Y. Z. Long, P. Jiang, T. Y. Zhang, B. Sun, *Nat. Commun.* **2020**, *11*, 3530.

[7] Y. T. Kwon, Y. S. Kim, S. Kwon, M. Mahmood, H. R. Lim, S. W. Park, S. O. Kang, J. J. Choi, R. Herbert, Y. C. Jang, Y. H. Choa, W. H. Yeo, *Nat. Commun.* **2020**, *11*, 3450.

[8] S. Mishra, Y.-S. Kim, J. Intarasirisawat, Y.-T. Kwon, Y. Lee, M. Mahmood, H.-R. Lim, R. Herbert, K. J. Yu, C. S. Ang, W.-H. Yeo, *Sci. Adv.* **2020**, *6*, eaay1729.

[9] S. Liu, K. Ma, B. Yang, H. Li, X. Tao, *Adv. Funct. Mater.* **2020**, *31*, 2007254.

[10] Y. Zhang, H. Wang, H. Lu, S. Li, Y. Zhang, *iScience* **2021**, *24*, 102716.

[11] J. Xiong, J. Chen, P. S. Lee, *Adv. Mater.* **2021**, *33*, 2002640.

[12] Q. Qiu, M. Zhu, Z. Li, K. Qiu, X. Liu, J. Yu, B. Ding, *Nano Energy* **2019**, *58*, 750.

[13] X. Shi, Y. Zuo, P. Zhai, J. Shen, Y. Yang, Z. Gao, M. Liao, J. Wu, J. Wang, X. Xu, Q. Tong, B. Zhang, B. Wang, X. Sun, L. Zhang, Q. Pei, D. Jin, P. Chen, H. Peng, *Nature* **2021**, *591*, 240.

[14] T. Huang, J. Zhang, B. Yu, H. Yu, H. Long, H. Wang, Q. Zhang, M. Zhu, *Nano Energy* **2019**, *58*, 375.

[15] S. Park, S. Ahn, J. Sun, D. Bhatia, D. Choi, K. S. Yang, J. Bae, J. J. Park, *Adv. Funct. Mater.* **2019**, *29*, 1808369.

[16] S. Dong, F. Xu, Y. Sheng, Z. Guo, X. Pu, Y. Liu, *Nano Energy* **2020**, *78*, 105327.

[17] L. Xu, H. Zhai, X. Chen, Y. Liu, M. Wang, Z. Liu, M. Umar, C. Ji, Z. Chen, L. Jin, Z. Liu, P. Yue, Y. Li, T. T. Ye, *Chem. Eng. J.* **2021**, *412*, 128639.

[18] L. Xu, Z. Liu, H. Zhai, X. Chen, R. Sun, S. Lyu, Y. Fan, Y. Yi, Z. Chen, L. Jin, J. Zhang, Y. Li, T. T. Ye, *ACS Appl. Mater. Interfaces* **2020**, *12*, 13265.

[19] J. Wang, J. He, L. Ma, Y. Zhang, L. Shen, S. Xiong, K. Li, M. Qu, *Chem. Eng. J.* **2020**, *390*, 124508.

[20] J. Qu, N. He, S. V. Patil, Y. Wang, D. Banerjee, W. Gao, *ACS Appl. Mater. Interfaces* **2019**, *11*, 14944.

[21] Z. Yang, Y. Pang, X. L. Han, Y. Yang, J. Ling, M. Jian, Y. Zhang, Y. Yang, T. L. Ren, *ACS Nano* **2018**, *12*, 9134.

[22] L. Lin, L. Wang, B. Li, J. Luo, X. Huang, Q. Gao, H. Xue, J. Gao, *Chem. Eng. J.* **2020**, *385*, 123391.

[23] S. Jang, J. Y. Choi, E. S. Yoo, D. Y. Lim, J. Y. Lee, J. K. Kim, C. Pang, *Composites, Part B* **2021**, *210*, 108674.

[24] S. Afroj, S. Tan, A. M. Abdelkader, K. S. Novoselov, N. Karim, *Adv. Funct. Mater.* **2020**, *30*, 2000293.

[25] Y. Khan, A. Thielens, S. Muin, J. Ting, C. Baumbauer, A. C. Arias, *Adv. Mater.* **2020**, *32*, 1905279.

[26] Q. Liu, B. Tian, J. Liang, W. Wu, *Mater. Horiz.* **2021**, *8*, 1634.

[27] H. Shahariar, I. Kim, H. Soewardiman, J. S. Jur, *ACS Appl. Mater. Interfaces* **2019**, *11*, 6208.

[28] R. Cao, X. Pu, X. Du, W. Yang, J. Wang, H. Guo, S. Zhao, Z. Yuan, C. Zhang, C. Li, Z. L. Wang, *ACS Nano* **2018**, *12*, 5190.

[29] T. Q. Trung, N. E. Lee, *Adv. Mater.* **2016**, *28*, 4338.

[30] H. Hong, J. Hu, X. Yan, *ACS Appl. Mater. Interfaces* **2019**, *11*, 27318.

[31] Q. Duan, Y. Lu, *ACS Appl. Mater. Interfaces* **2021**, *13*, 28832.

[32] L. Wang, X. Fu, J. He, X. Shi, T. Chen, P. Chen, B. Wang, H. Peng, *Adv. Mater.* **2020**, *32*, 1901971.

[33] H. Jin, N. Matsuhisa, S. Lee, M. Abbas, T. Yokota, T. Someya, *Adv. Mater.* **2017**, *29*, 1605848.

[34] M. Tang, P. Zheng, Y. Wu, P. Zhu, Y. Qin, Y. Jiang, R. Sun, C. P. Wong, Z. Li, *Compos. Commun.* **2020**, *19*, 121.

[35] J. Liang, C. Jiang, W. Wu, *Appl. Phys. Rev.* **2021**, *8*, 021319.

[36] X. Zhang, X. Wang, Z. Lei, L. Wang, M. Tian, S. Zhu, H. Xiao, X. Tang, L. Qu, *ACS Appl. Mater. Interfaces* **2020**, *12*, 14459.

[37] J. Luo, S. Gao, H. Luo, L. Wang, X. Huang, Z. Guo, X. Lai, L. Lin, R. K. Y. Li, J. Gao, *Chem. Eng. J.* **2021**, *406*, 126898.

[38] F. Marra, S. Minutillo, A. Tamburrano, M. S. Sarto, *Mater. Des.* **2021**, *198*, 109306.

[39] B. Wang, K. Yang, H. Cheng, T. Ye, C. Wang, *Chem. Eng. J.* **2021**, *404*, 126393.

[40] X. Shi, S. Liu, Y. Sun, J. Liang, Y. Chen, *Adv. Funct. Mater.* **2018**, *28*, 1800850.

[41] X. Shi, H. Wang, X. Xie, Q. Xue, J. Zhang, S. Kang, C. Wang, J. Liang, Y. Chen, *ACS Nano* **2018**, *13*, 649.

[42] L. Duan, D. R. D'Hooge, L. Cardon, *Prog. Mater. Sci.* **2020**, *114*, 100617.

[43] S. G. Yoon, H. J. Koo, S. T. Chang, *ACS Appl. Mater. Interfaces* **2015**, *7*, 27562.

[44] B. Niu, S. Yang, T. Hua, X. Tian, M. Koo, *Nano Res.* **2020**, *14*, 1043.

[45] S. Yang, C. Li, X. Chen, Y. Zhao, H. Zhang, N. Wen, Z. Fan, L. Pan, *ACS Appl. Mater. Interfaces* **2020**, *12*, 19874.

[46] S. Yao, J. Yang, F. R. Poblete, X. Hu, Y. Zhu, *ACS Appl. Mater. Interfaces* **2019**, *11*, 31028.